Acoustic Waves Induced by Einstein–de Haas Effect in the Ultrafast Core Reversal of Magnetic Vortex

Jiajun Sun,[1] Shengbin Shi,[1] and Jie Wang[1,2,3,*]
[1]Department of Engineering Mechanics, Zhejiang University, Zheda Road 38, Hangzhou, Zhejiang 310027, China
[2]Zhejiang Laboratory, Hangzhou, Zhejiang 311100, China
[3]Key Laboratory of Soft Machines and Smart Devices of Zhejiang Province, Zheda Road 38, Hangzhou, Zhejiang 310027, China

(Received 22 August 2022; accepted 19 May 2023; published 22 June 2023)

The interaction between acoustic wave and magnetization in ferromagnetic thin films has attracted great attention due to its interesting physics and potential applications. However, up to now, the magneto-acoustic interaction has mainly been studied on the basis of magnetostriction. In this Letter, we develop a phase field model of magneto-acoustic interaction based on the Einstein–de Haas effect, and predict the acoustic wave during the ultrafast core reversal of magnetic vortex in a ferromagnetic disk. Because of the Einstein–de Haas effect, the ultrafast change of magnetization at the vortex core leads to a large mechanical angular momentum, which induces a body couple at the vortex core and excites a high-frequency acoustic wave. Moreover, the displacement amplitude of the acoustic wave is highly dependent on the gyromagnetic ratio. The smaller the gyromagnetic ratio is, the larger the displacement amplitude is. The present work not only provides a new mechanism for dynamic magnetoelastic coupling but also sheds new insights on the magneto-acoustic interaction.

DOI: 10.1103/PhysRevLett.130.256701

The Einstein–de Haas effect refers to a phenomenon of mechanical rotation caused by the change of magnetization, in which the lost magnetic angular momentum is converted into mechanical angular momentum [1]. The early Einstein–de Haas experiments were only carried out on macroscopic samples, which were used to measure the gyromagnetic ratio for various magnetic materials [2]. In recent years, the progress in the manufacturing and measuring of microscopic magnet revives interest in the quantum Einstein–de Haas effect of single-molecule magnet [3,4] as well as the ultrafast Einstein–de Haas effect [5,6]. Although the microscopic mechanism of the mutual conversion between magnetic angular momentum and mechanical angular momentum is controversial, different theoretical models have been established to describe the Einstein–de Haas effect [7–10].

According to the theoretical models, the Einstein–de Haas effect depends on the change rate of magnetization. The larger the change rate is, the stronger the Einstein–de Haas effect is. Because of the large change rate of magnetization, the ultrafast demagnetization induced by femtosecond laser exhibits very strong Einstein–de Haas effect [11]. Similar to the ultrafast demagnetization, the ultrafast core reversal of a magnetic vortex could also provide a large change rate of local magnetization at the vortex core [12,13], which holds a promise to generate strong Einstein–de Haas effect. Recently, the ultrafast core reversal of a magnetic vortex has been investigated extensively [14], including the spin-wave-mediated core reversal [15], fast core reversal at high temperature [16], unidirectional core reversal under magnetic pulse [17], periodic core reversal under alternating magnetic field [18], deterministic vortex reversal by pulsed electric field-induced strain [19] and ultrafast core reversal by a local field pulse [20]. The ultrafast core reversal of magnetic vortex is not only important for its application in information storage unit [21], but also can be used to excite spin waves [22]. The spin wave can be regarded as a collective precession of magnetization [23–25], which can excite acoustic waves through magneto-acoustic interaction [9,26–30].

In recent years, the study of magneto-acoustic interaction has mainly focused on the spin-wave resonance driven by the acoustic-wave in multiferroic systems [31–37] as well as the remote control of magnetic bits through surface acoustic wave [38]. In previous work, the magneto-acoustic interaction has been studied mainly on the basis of magnetostriction, in which the Einstein–de Haas effect is excluded. For the ultrafast core reversal of a magnetic vortex in Fig. 1(a), the change of local magnetization at the core is ultrafast. Therefore, the Einstein–de Haas effect is strong and cannot be neglected. According to the Einstein–de Haas effect, there is mutual conversion between magnetic angular momentum and mechanical angular momentum during the ultrafast core reversal of magnetic vortex, resulting in a mechanical couple at the vortex core as shown in Fig. 1(b). Although strong radiation of the spin wave from the dynamic core of magnetic vortex was found in magnetic thin films [22,39,40], it is still unknown whether the ultrafast core reversal of magnetic vortex can excite an acoustic wave as shown in Fig. 1(c).

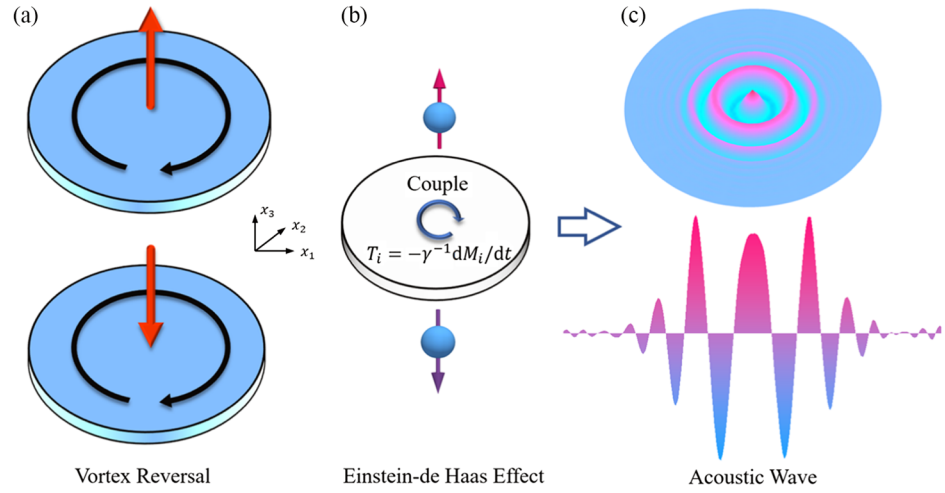

FIG. 1. (a) Schematic illustration of the magnetization reversal at the vortex core in a ferromagnetic disk. (b) A body couple T_i generated at the vortex core by the magnetization reversal due to the Einstein–de Haas effect. (c) The rapid appearance of the body couple at the vortex core induces high-frequency acoustic waves in the ferromagnetic disk.

In this Letter, we develop a dynamic phase field model for magneto-acoustic interaction by combining the Einstein–de Haas effect and generalized elastodynamics equation with Landau-Lifshitz-Gilbert equation. Different from the traditional magnetoelastic coupling of magnetization and strain [41,42], the coupling between the body couple and the change rate of magnetization, i.e., the Einstein–de Haas effect, is employed in the present model to describe the magneto-acoustic interaction. In order to model the dynamic magnetoelastic coupling behavior caused by a spatially nonuniform change of spin angular momentum, the couple stresses and the body couple are introduced into the elastodynamic equation of the phase field model. The phase field simulations show that the acoustic waves are excited due to the Einstein–de Haas effect during the ultrafast core reversal of magnetic vortex. Furthermore, the dependence of the displacement amplitude of the acoustic wave on gyromagnetic ratio is revealed and its implication in the measurement of gyromagnetic ratio is also discussed.

In the phase field model, the Einstein–de Haas effect is considered in the coupled form of the magnetization change rate and the body couple as [5]

$$T_i = -\frac{\gamma^{-1} dM_i}{dt} \quad (i = 1, 2, 3), \tag{1}$$

where T_i is the component of body couple, M_i is the component of magnetization vector, t is the time, and γ is the gyromagnetic ratio. Equation (1) shows that the change of magnetic angular momentum dM_i leads to a change in mechanical angular momentum $T_i dt$, in which the conservation of total angular momentum is satisfied.

When the body couple induced by magnetization change is considered, the conventional mechanical equilibrium equation of $\sigma_{ji,j} = \rho \partial u_i^2 / \partial t^2$ is not applicable due to the absence of couple stress, and thus a generalized mechanical equilibrium equation with couple stress and body couple is needed [43]. The generalized mechanical equilibrium equation can be expressed as

$$\sigma_{ji,j} + \frac{1}{2} e_{ikr} q_{sr,sk} + \frac{1}{2} e_{isr} T_{r,s} + F_i = \rho \frac{\partial^2 u_i}{\partial t^2}, \tag{2}$$

where σ_{ji} is the symmetric stress tensor, the subscript of, j represents the derivative of the variables with respect to the coordinate of x_j, e_{ikr} is the permutation tensor, q_{sr} is the couple stress tensor, F_i is the component of body force, ρ is the mass density of the material, and u_i is the component of displacement. In Eq. (2), Einstein's summation convention is employed and all the subscripts of i, j, k, r and s take the number of 1, 2 and 3. Based on the constitutive law of anisotropic materials, the stress tensor can be expressed as $\sigma_{ij} = c_{ijkl} \varepsilon_{kl}$, in which c_{ijkl} are the elastic constant tensor and $\varepsilon_{ij} = \frac{1}{2}(u_{i,j} + u_{j,i})$ is the strain tensor.

Based on the theory of elasticity [44], the coupling stress is related to the curvature tensor by the constitutive law of $q_{ij} = 2G l_e^2 \chi_{ij}$, in which G is the shear modulus, χ_{ij} is the curvature tensor, and l_e is the material length scale parameter. The curvature tensor can be expressed by displacement components as $\chi_{ij} = \frac{1}{4}(e_{jkl} u_{l,ki} + e_{ikl} u_{l,kj})$. If the couple stress tensor and body couple are removed, Eq. (2) is reduced to the equilibrium equation of conventional elasticity theory. Substituting the body couple of Eq. (1) into the equilibrium equation of Eq. (2), the elasticity theory has been generalized to include the Einstein–de Haas effect, which is able to model the elastic dynamic deformation of ferromagnetic materials due to the body couple.

The temporal evolution of magnetization vector $\boldsymbol{M}$ in ferromagnetic materials is described by the Landau-Lifshitz-Gilbert (LLG) equation as

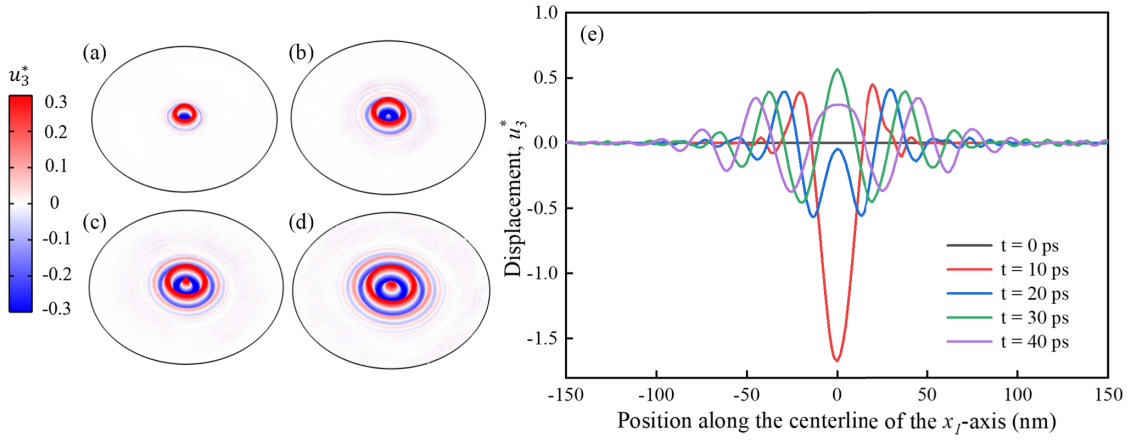

FIG. 2. The contour map of out-of-plane displacement of u_3^* for the FeGa ferromagnetic disk at different time with (a) $t = 10$, (b) $t = 20$ (c) $t = 30$, and (d) $t = 40$ ps. (e) The displacement profiles of u_3^* on the center line of the disk at different times. The axisymmetric acoustic wave propagates outward from the center of the disk, which is induced by the couple at the center due to the Einstein–de Haas effect.

$$\frac{\partial \boldsymbol{M}}{\partial t} = -\gamma \boldsymbol{M} \times \boldsymbol{H}_{\text{eff}} + \frac{\alpha}{M_s} \boldsymbol{M} \times \frac{\partial \boldsymbol{M}}{\partial t}, \tag{3}$$

in which α is the Gilbert damping constant, M_s is the saturation magnetization, $\boldsymbol{H}_{\text{eff}} = -(1/\mu_0)(\delta F/\delta M)$ is the effective magnetic field and μ_0 is the permeability of free space. The total free energy F can be obtained by integrating the free energy density over the entire volume as $F = \int f dV$ and f is the total free-energy density that is given in the Supplemental Material [45]. In addition to LLG and mechanical equilibrium equation, the Maxwell equation of

$$\frac{\partial}{\partial x_i}\left(-\frac{\partial f}{\partial H_i}\right) = 0 \tag{4}$$

is solved to obtain the magnetostatic potential and magnetic field, in which $H = -\nabla\phi$ is the magnetic field and ϕ is the magnetic potential [53–55]. To simulate the full coupled evolution of displacement and magnetization during vortex core reversal in the ferromagnetic disk, a nonlinear finite element method is adopted to numerically solve the coupled governing equations of Eqs. (2)–(4). The detailed solution procedure and the used material parameters are given in the Supplemental Material [45]. In our research, the external magnetic field in the vortex core area is very large, so the magnetostatic field can be ignored, while for the outside region without external magnetic field, the demagnetizing field can be obtained by solving the Maxwell equation.

Using the proposed phase field model, a magnetic vortex with downward core is predicted for a ferromagnetic FeGa disk with the radius of 200 nm and the thickness of 2 nm, as shown in Fig. S1(a) in the Supplemental Material [45]. In order to achieve a wave propagating from the center to outside, a local magnetic field of $H_3 = 5 \times 10^6$ A/m is applied along the x_3 direction at the center circle with a radius of 10 nm, which can avoid large-scale magnetization reversal and complex dynamic coupling. In practice, the local magnetic field could be applied by a saturated magnetic probe of a magnetic force microscope [56–58].

After 5 ps, the vortex core is reversed from downward to upward under the magnetic field, as shown in Fig. S1(b) [45]. Because of the Einstein–de Haas effect, the magnetization reversal at the vortex core generates a localized body couple at ultrashort time, which triggers acoustic waves in the ferromagnetic disk as shown in Fig. 2. Figures 2(a)–2(d) give the contour maps of out-of-plane displacement of u_3^* on the upper surface of the ferromagnetic disk at different time from 10 to 40 ps. The displacement is normalized by $u_3^* = u_3/u_0$ with $u_0 = 1 \times 10^{-12}$ m, which is the same order as the experimental observation [5].

From the contour maps, it can be found the propagation direction of out-of-plane displacement is perpendicular to the displacement direction, indicating it is a transversal acoustic wave. The axisymmetric propagation of the acoustic wave is also shown by the profiles of displacement on the centerline of the disk at different time in Fig. 2(e). With the evolution of time, the displacement at the center changes from downward to upward. Based on the position of the wave front at different time, the velocity of the acoustic wave is calculated as 4300 m/s, which is close to that calculated from the theory of elasticity. In order to understand the drastic change of the magnetization and displacement, the distribution of u_3^* and M_3 within the first 14 ps are shown in Fig. S2 and the coupling dynamics are shown in Fig. S3 in which the fluctuation of displacement is more obvious than that of magnetization. Additionally, we conducted a comparative study on different magnetic damping constants, as shown in Fig. S4 [45]. In order to reduce the influence of the propagation of the spin wave, we adopt a large magnetic damping $\alpha = 0.5$ in our

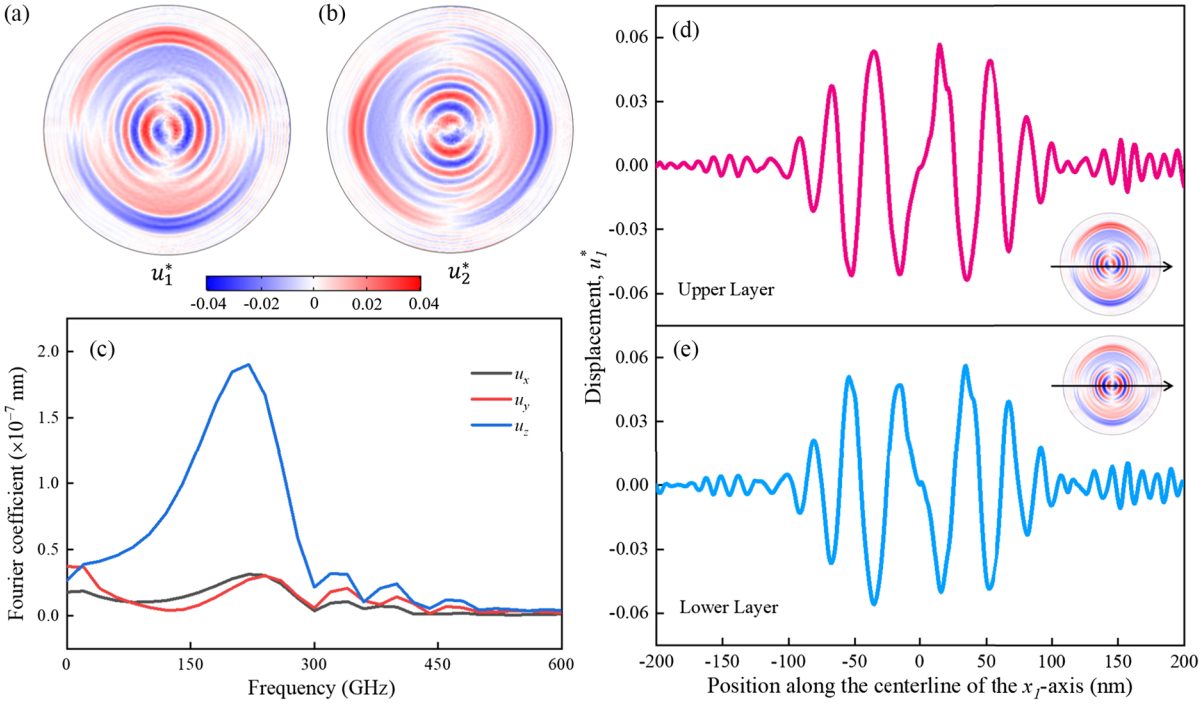

FIG. 3. The contour map of in-plane displacements of (a) u_1^* and (b) u_2^* for the FeGa ferromagnetic disk at the time of $t = 40$ ps. (c) Frequency spectrum diagram of acoustic waves at different directions. The displacement component of u_1^* on the upper surface (d) and (e) the lower surface of the disk along the center line of the x_1 axis at $t = 40$ ps. The black arrows in the insets denote the location of the center line. The directions of displacement of the two surfaces are opposite at the same location on the x_1 axis.

simulation. The inconspicuous fluctuation of magnetization is due to the relatively large magnetic damping. It should be noted that the thickness of the thin film may affect the frequency, amplitude, and mode of acoustic waves. In general, thinner films tend to generate acoustic waves with out-of-plane displacement as shown in the present work.

In addition to out-of-plane displacement, in-plane displacements of u_1^* and u_2^* are also excited by Einstein–de Haas (EdH) effect as shown in Figs. 3(a) and 3(b), which is collected on the upper surface of the ferromagnetic disk at $t = 40$ ps. Based on the contour maps, the components of u_1^* and u_2^* outside the core is almost perpendicular to the radial direction. In order to distinguish the magnetostriction and EdH effect, the phase field simulations on the same system with only the magnetostriction and with both magnetostriction and EdH effect are conducted with the formula of Sec. II in the Supplemental Material [45]. The simulation results are given in Fig. S6, indicating that magnetostriction almost plays no role in generating the acoustic waves.

In order to understand the dynamic characteristics of the excited acoustic waves, FFT spectrum analysis is conducted for the volume-averaged displacements of the disk in the period of time from 0 to 50 ps. Figure 3(c) shows the frequency spectrum diagram of three displacements. In the frequency spectrum diagram, the frequency at the first peak of spectrum curve of out-of-plane displacement is different from that of in-plane displacement, indicating that out-of-plane displacement and in-plane displacement belong to two different acoustic waves. There are also several small peaks in the frequency spectrum curves for both in-plane and out-of-plane displacements which indicate the existence of high frequency acoustic waves.

The Fourier coefficient of out-of-plane displacement at first peak is much larger than that of in-plane displacement, which is consistent with the result that the maximum amplitude of out-of-plane wave in Fig. 2(e) is one order larger than the in-plane wave in Fig. 3(d). Figure 3(e) gives in-plane displacement on the lower surface of the disk. Comparing in-plane displacements on the upper and lower surfaces in Figs. 3(d) and 3(e), the displacements of two surfaces are opposite at the same location on the x_1 axis. Moreover, the displacement distribution along the thickness direction of the disk is antisymmetric with respect to the middle plane, which implies the deformation of the middle plane of the disk is trivial.

It is interesting that the displacements of the in-plane acoustic wave in Fig. 3 are almost antisymmetric with respect to the center point of the center line, which is totally different from the symmetric distribution of displacement of the out-of-plane acoustic wave in Fig. 2. The antisymmetric distribution of displacement persists during the wave propagation as shown by the profiles of in-plane displacements along the center line of the x_1 axis at different time in

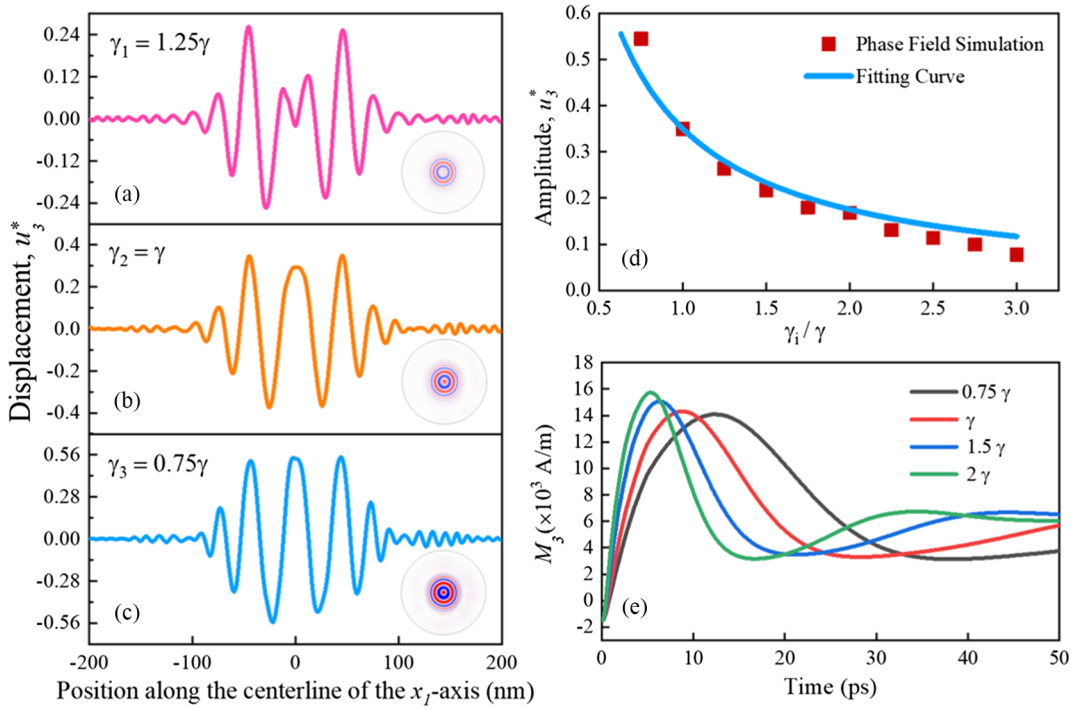

FIG. 4. The curves of displacement u_3^* along the center line of the x_1 axis at $t = 40$ ps with different gyromagnetic ratios (a) $\gamma_1 = 1.25\gamma$ (b) $\gamma_2 = \gamma$, and (c) $\gamma_3 = 0.75\gamma$. The insets show the contour map of displacement component of u_3^*. The smaller the gyromagnetic ratio is, the larger the displacement amplitude is. (d) The maximum amplitude of displacement u_3^* at $t = 40$ ps with different gyromagnetic ratios. An explicit inverse relation between the displacement amplitude and gyromagnetic ratio is obtained as $u_3^* = [a/(\gamma_i/\gamma)]$ with $a = 3.5 \times 10^{-4}$ (solid line) by fitting the simulation data (square dots). (e) The volume-averaged magnetization component M_3 of the ferromagnetic disk with different gyromagnetic ratios.

Fig. S5 [45]. The out-of-plane body couple screws the disk at the center and induces a circle wave in the plane of the disk. Because of the rotation nature of a circle wave, the distribution of displacement of in-plane waves is antisymmetric.

Next, we investigate the influence of the gyromagnetic ratio on the acoustic wave. Figures 4(a)–4(c) show the curves of displacement u_3^* along the center line of the x_1 axis at $t = 40$ ps with different gyromagnetic ratios. The insets show the contour map of displacement u_3^*. It is found that the fluctuations of displacement are similar for different gyromagnetic ratios, while the amplitudes are different. The smaller the gyromagnetic ratio is, the larger the displacement amplitude is, which is confirmed by the contour map of out-of-plane displacement in the insets of Figs. 4(a)–4(c). In the same color range, the contour with the smaller gyromagnetic ratio 0.75γ is darker. In order to deeply understand the effect of gyromagnetic ratio on acoustic waves, multiple sets of simulations with different gyromagnetic ratios are conducted. The gyromagnetic ratio changes from 0.75γ to 3γ and the corresponding displacement amplitude are calculated and plotted by the square dots in Fig. 4(d). The displacement amplitude changes dramatically when the gyromagnetic ratio changes from 0.75γ to γ. When the gyromagnetic ratio is larger than γ, the displacement amplitude decreases moderately with the increase of the gyromagnetic ratio. The change rate of displacement amplitude with small gyromagnetic ratio is much larger than that with large gyromagnetic ratio. Based on the simulated displacement amplitudes at different gyromagnetic ratios, an explicit inverse relation between the displacement amplitude u_3^* and gyromagnetic ratio γ_i is obtained as $u_3^* = [a/(\gamma_i/\gamma)]$ with $a = 3.5 \times 10^{-4}$ by least square fitting, as shown by the solid line in Fig. 4(d). This result is consistent with the definition of the Einstein–de Haas effect of Eq. (1), in which the magnitude of the body couple is inversely proportional to the gyromagnetic ratio. Based on the relationship of mechanical torque and gyromagnetic ratio, the Einstein–de Haas effect has been employed to measure the gyromagnetic ratio through the macroscopic magnetomechanical experiments in 1966 [2]. Similarly, based on the microscopic Einstein–de Haas effect, the gyromagnetic ratio can be determined by measuring the displacement of acoustic waves because the displacement has an explicit relationship with the gyromagnetic ratio.

The gyromagnetic ratio not only affects the displacement amplitude of the acoustic wave through the Einstein–de Haas effect, but also has great influence on the evolution of magnetization through the LLG equation. Based on LLG

equation, the gyromagnetic ratio is related to the precession process of the magnetization, so the magnetization evolutions are different for different gyromagnetic ratios, as shown in Fig. 4(e). Generally, the smaller the gyromagnetic ratio is, the smaller the magnetization change is. According to Eq. (1), the body couple is proportional to the change rate of magnetization. When the gyromagnetic ratio becomes smaller, although the change of magnetization becomes slower, the body couple becomes larger. These results indicate that the magnetization change rate induced by the gyromagnetic ratio is relatively small and has less effect on the body couple comparing to the direction effect of gyromagnetic ratio on body couple.

In conclusion, a phase field model is proposed to predict the coupling evolution of magnetization and displacement in ferromagnetic materials based on the Einstein–de Haas effect and generalized elastodynamics with couple stress. Different from the traditional magnetoelastic coupling of magnetization and strain, the coupling between the body couple and the change rate of magnetization is considered in the phase field model. The ultrafast core reversal of magnetic vortex in a FeGa disk is simulated by the phase field model. Because of the Einstein–de Haas effect, the change of magnetic angular momentum during core reversal leads to a change in mechanical angular momentum, resulting in a large body couple at the vortex core and excites high-frequency acoustic waves. It is found that the displacement amplitude of acoustic waves is highly dependent on the gyromagnetic ratio. The smaller the gyromagnetic ratio is, the larger the displacement amplitude is. This work not only suggests that acoustic wave can be generated through a novel magnetoelastic coupling in ferromagnetic thin films but also sheds new insights on the magneto-acoustic interaction.

This work was financially supported by the National Program on Key Basic Research Project (Grant No. 2022YFB3807601), the National Natural Science Foundation of China (Grants No. 11972320, No. 12192214, No. 12272338) and the Key Research Project of Zhejiang Laboratory (Grant No. 2021 PE0AC02).

*jw@zju.edu.cn

[1] A. Einstein and W. J. de Haas, Experimental proof of the existence of Ampère's molecular currents, in *KNAW, Proceedings, Amsterdam* (1915), pp. 696–711.
[2] G. G. Scott, Phys. Rev. **148**, 525 (1966).
[3] W. Izumida, R. Okuyama, K. Sato, T. Kato, and M. Matsuo, Phys. Rev. Lett. **128**, 017701 (2022).
[4] M. Ganzhorn, S. Klyatskaya, M. Ruben, and W. Wernsdorfer, Nat. Commun. **7**, 11443 (2016).
[5] C. Dornes *et al.*, Nature (London) **565**, 209 (2019).
[6] S. R. Tauchert *et al.*, Nature (London) **602**, 73 (2022).
[7] T. Wells, A. P. Horsfield, W. M. C. Foulkes, and S. L. Dudarev, J. Chem. Phys. **150**, 224109 (2019).
[8] R. Jaafar, E. M. Chudnovsky, and D. A. Garanin, Phys. Rev. B **79**, 104410 (2009).
[9] R. Zarzuela and E. M. Chudnovsky, J. Supercond. Novel Magn. **28**, 3411 (2015).
[10] L. Zhang and Q. Niu, Phys. Rev. Lett. **112**, 085503 (2014).
[11] M. Hennecke, I. Radu, R. Abrudan, T. Kachel, K. Holldack, R. Mitzner, A. Tsukamoto, and S. Eisebitt, Phys. Rev. Lett. **122**, 157202 (2019).
[12] R. Hertel, S. Gliga, M. Fähnle, and C. M. Schneider, Phys. Rev. Lett. **98**, 117201 (2007).
[13] K. Y. Guslienko, K. S. Lee, and S. K. Kim, Phys. Rev. Lett. **100**, 027203 (2008).
[14] Y. Zheng and W. J. Chen, Rep. Prog. Phys. **80**, 086501 (2017).
[15] M. Kammerer, H. Stoll, M. Noske, M. Sproll, M. Weigand, C. Illg, G. Woltersdorf, M. Fähnle, C. Back, and G. Schütz, Phys. Rev. B **86**, 134426 (2012).
[16] K. M. Lebecki and D. Legut, J. Magn. Magn. Mater. **411**, 7 (2016).
[17] M. Noske *et al.*, Phys. Rev. B **90**, 104415 (2014).
[18] X. P. Ma, M. X. Cai, P. Li, J. H. Shim, H. G. Piao, and D. H. Kim, J. Magn. Magn. Mater. **502**, 166481 (2020).
[19] Y. Zhang *et al.*, Sci. Bull. **65**, 1260 (2020).
[20] R. Rückriem, T. Schrefl, and M. Albrecht, Appl. Phys. Lett. **104**, 052414 (2014).
[21] K. Yamada, S. Kasai, Y. Nakatani, K. Kobayashi, H. Kohno, A. Thiaville, and T. Ono, Nat. Mater. **6**, 270 (2007).
[22] S. Choi, K. S. Lee, K. Y. Guslienko, and S. K. Kim, Phys. Rev. Lett. **98**, 087205 (2007).
[23] G. Dieterle *et al.*, Phys. Rev. Lett. **122**, 117202 (2019).
[24] M. Geilen *et al.*, Appl. Phys. Lett. **120**, 242404 (2021).
[25] J. Sun, S. Shi, and J. Wang, Adv. Eng. Mater. **24**, 2101245 (2022).
[26] S. Tateno, Y. Kurimune, M. Matsuo, K. Yamanoi, and Y. Nozaki, Phys. Rev. B **104**, L020404 (2021).
[27] P. Delsing and A. N. Cleland, J. Phys. D: Appl. Phys. **52**, 353001 (2019).
[28] J. Holanda, D. S. Maior, A. Azevedo, and S. M. Rezende, Nat. Phys. **14**, 500 (2018).
[29] T. Funato and M. Matsuo, Phys. Rev. Lett. **128**, 077201 (2022).
[30] J. Sun, Y. Zhao, S. Shi, Y. Zhang, and J. Wang, Appl. Phys. Lett. **121**, 242406 (2022).
[31] J. Y. Duquesne, P. Rovillain, C. Hepburn, M. Eddrief, P. Atkinson, A. Anane, R. Ranchal, and M. Marangolo, Phys. Rev. Appl. **12**, 024042 (2019).
[32] M. Weiler, L. Dreher, C. Heeg, H. Huebl, R. Gross, M. S. Brandt, and S. T. B. Goennenwein, Phys. Rev. Lett. **106**, 117601 (2011).
[33] P. G. Gowtham, T. Moriyama, D. C. Ralph, and R. A. Buhrman, J. Appl. Phys. **118**, 233910 (2015).
[34] L. Dreher, M. Weiler, M. Pernpeintner, H. Huebl, R. Gross, M. S. Brandt, and S. T. B. Goennenwein, Phys. Rev. B **86**, 134415 (2012).
[35] M. Weiler, H. Huebl, F. S. Goerg, F. D. Czeschka, R. Gross, and S. T. B. Goennenwein, Phys. Rev. Lett. **108**, 176601 (2012).
[36] J. M. Hu, G. Sheng, J. X. Zhang, C. W. Nan, and L. Q. Chen, Appl. Phys. Lett. **98**, 112505 (2011).

[37] F. Mahfouzi and N. Kioussis, Phys. Rev. Lett. **128**, 215902 (2022).
[38] V. S. Vlasov, A. M. Lomonosov, A. V. Golov, L. N. Kotov, V. Besse, A. Alekhin, D. A. Kuzmin, I. V. Bychkov, and V. V. Temnov, Phys. Rev. B **101**, 024425 (2020).
[39] C. Behncke, C. F. Adolff, N. Lenzing, M. Hänze, B. Schulte, M. Weigand, G. Schütz, and G. Meier, Commun. Phys. **1**, 50 (2018).
[40] K. S. Lee, S. Choi, and S. K. Kim, Appl. Phys. Lett. **87**, 192502 (2005).
[41] A. H. Reid *et al.*, Nat. Commun. **9**, 388 (2018).
[42] J. Wang, Annu. Rev. Mater. Res. **49**, 361 (2019).
[43] A. R. Hadjesfandiari and G. F. Dargush, Int. J. Solids Struct. **48**, 2496 (2011).
[44] D. C. C. Lam, F. Yang, A. C. M. Chong, J. Wang, and P. Tong, J. Mech. Phys. Solids **51**, 1477 (2003).
[45] See Supplemental Material at http://link.aps.org/supplemental/10.1103/PhysRevLett.130.256701 for the finite element implementation of the phase field model based on the Einstein–de Haas effect and ordinary magnetostriction effect, the material parameters, the detailed discussion of the displacements and magnetization, the comparison of displacements with the Einstein–de Haas effect and ordinary magnetostriction effect, which includes Refs. [46–52].
[46] COMSOL Multiphysics, http://comsol.com.
[47] C. M. Landis, J. Mech. Phys. Solids **56**, 3059 (2008).
[48] H. H. Wu, Y. Ke, J. Zhu, Z. Wu, and X. L. Wang, J. Phys. D: Appl. Phys. **54**, 155301 (2021).
[49] J. X. Zhang and L. Q. Chen, Acta Mater. **53**, 2845 (2005).
[50] C. Y. Liang, S. M. Keller, A. E. Sepulveda, A. Bur, W. Y. Sun, K. Wetzlar, and G. P. Carman, Nanotechnology **25**, 435701 (2014).
[51] J. Wang, G. P. Li, T. Shimada, H. Fang, and T. Kitamura, Appl. Phys. Lett. **103**, 242413 (2013).
[52] F. Alloys, A. E. Clark, J. B. Restorff, M. Wun-fogle, T. A. Lograsso, and D. L. Schlagel, IEEE Trans. Magn. **36**, 3238 (2000).
[53] J. Wang and J. Zhang, Int. J. Solids Struct. **50**, 3597 (2013).
[54] J. Sun, Y. Zhang, and J. Wang, Int. J. Solids Struct. **233**, 111213 (2021).
[55] J. Sun, S. Shi, Y. Wang, and J. Wang, Acta Mech. **234**, 283 (2023).
[56] A. Casiraghi, H. Corte-León, M. Vafaee, F. Garcia-Sanchez, G. Durin, M. Pasquale, G. Jakob, M. Kläui, and O. Kazakova, Commun. Phys. **2**, 145 (2019).
[57] W. M. Ju, J. E. Bickel, N. Pradhan, K. E. Aidala, and M. Tuominen, Nanotechnology **31**, 115205 (2020).
[58] Y. Wang, J. Sun, T. Shimada, H. Hirakata, T. Kitamura, and J. Wang, Phys. Rev. B **102**, 014440 (2020).